



HAL
open science

Reactivity of unactivated peroxymonosulfate with nitrogenous compounds

Maolida Nihemaiti, Ratish Ramyad Permala, Jean-Philippe Croué

► To cite this version:

Maolida Nihemaiti, Ratish Ramyad Permala, Jean-Philippe Croué. Reactivity of unactivated peroxymonosulfate with nitrogenous compounds. *Water Research*, 2020, 169, pp.115221 -. 10.1016/j.watres.2019.115221 . hal-03488542

HAL Id: hal-03488542

<https://hal.science/hal-03488542>

Submitted on 21 Dec 2021

HAL is a multi-disciplinary open access archive for the deposit and dissemination of scientific research documents, whether they are published or not. The documents may come from teaching and research institutions in France or abroad, or from public or private research centers.

L'archive ouverte pluridisciplinaire **HAL**, est destinée au dépôt et à la diffusion de documents scientifiques de niveau recherche, publiés ou non, émanant des établissements d'enseignement et de recherche français ou étrangers, des laboratoires publics ou privés.



Distributed under a Creative Commons Attribution - NonCommercial 4.0 International License

14 **Abstract**

15 A recent investigation has demonstrated that peroxymonosulfate (PMS), a peroxide
16 commonly applied as a radical precursor during advanced oxidation processes (AOPs), can
17 degrade organic contaminants without the involvement of radicals. However, little is known
18 about this non-radical reaction mechanism. In this study, the reactivity of PMS with several
19 nitrogenous compounds was investigated. Fluoroquinolone antibiotics (except for flumequine)
20 were rapidly degraded by direct PMS oxidation, followed by aliphatic amines (e.g.,
21 metoprolol and venlafaxine) and nitrogenous heterocyclic compounds (e.g., adenine and
22 caffeine) at pH 8. The degradation rate of fluoroquinolones followed a second-order kinetic
23 and was highly pH and structure-dependent. Unlike the radical-based AOPs, the direct
24 degradation of contaminants by PMS was less influenced by the scavenging effect of the
25 water matrix. High-Resolution Mass Spectrometry (HRMS) analysis demonstrated that the
26 piperazine ring of fluoroquinolones was the main reaction site. Results showed that the direct
27 electron-transfer from nitrogenous moieties (piperazine ring) to PMS can produce amide and
28 aldehyde compounds. An amide-containing transformation product of ciprofloxacin (m/z 320),
29 showing the highest signal intensity on HRMS, was previously recorded during ozonation.
30 Moreover, the hydroxylamine analogue of ciprofloxacin and enrofloxacin *N*-oxide were
31 tentatively identified, and the formation of the latter was not impacted by the dissolved
32 oxygen in water. These results suggested that PMS also reacts with nitrogenous compounds
33 via oxygen transfer pathway. Agar disk-diffusion tests indicated that PMS treatment
34 efficiently removed the antibacterial activity of ciprofloxacin with the complete degradation
35 of parent antibiotic, except for the transformation products in an earlier stage, which might
36 still exert antibacterial potency.

37 **Keywords**

38 Peroxymonosulfate, nitrogenous compounds, high-resolution mass spectrometry, reaction
39 mechanism

40 **Abbreviations**

41	AOPs	Advanced Oxidation Processes
42	CIP	Ciprofloxacin
43	<i>D</i>	Distribution Coefficient
44	<i>E. coli</i> B	<i>Escherichia. Coli</i> B
45	ENR	Enrofloxacin
46	HPLC	High-Performance Liquid Chromatography
47	HRMS	High-Resolution Mass Spectrometry
48	LC	Liquid Chromatography
49	NOM	Natural Organic Matter
50	PDS	Peroxydisulfate
51	PMS	Peroxymonosulfate

52 **1. Introduction**

53 Advanced Oxidation Processes (AOPs) have gained increasing interest in recent years for the
54 removal of refractory contaminants during water treatment and soil remediation. Hydrogen
55 peroxide (H_2O_2), peroxydisulfate ($\text{S}_2\text{O}_8^{2-}$, PDS), and peroxymonosulfate (HSO_5^- , PMS) are
56 the commonly used peroxides for AOPs. The activation of these peroxides by energy (e.g.,
57 UV irradiation) and electron transfer (e.g., transition metal-based catalysis) generates strong
58 oxidizing species such as hydroxyl radical ($\cdot\text{OH}$, 1.9–2.7 V) and sulfate radical ($\text{SO}_4^{\cdot-}$,
59 2.5–3.1 V) (Neta et al., 1988). Many studies have demonstrated that $\cdot\text{OH}$ and $\text{SO}_4^{\cdot-}$ have high
60 potential to eliminate pharmaceuticals, pesticides, and industrial contaminants (Lutze et al.,
61 2015; Wols et al., 2015). However, certain water matrix components (e.g., organic matter,
62 bicarbonate, and halides) are known to reduce the efficiency of AOPs by significantly
63 scavenging the radicals (Zhang et al., 2013; Yang et al., 2016b). Moreover, the leaching of
64 heavy metal (e.g., cobalt) can be an important issue during transition metal-based AOPs (Ike
65 et al., 2018).

66 PMS is commercially available and known as Oxone ($2\text{KHSO}_5 \cdot \text{KHSO}_4 \cdot \text{K}_2\text{SO}_4$). It is
67 relatively stable, thus convenient for storage and transportation. PMS has been applied as a
68 non-chlorine disinfectant in swimming pools and for delignification in paper and pulp
69 industry. The electron-transfer from transition metal-based catalysts (e.g., cobalt, copper, iron)
70 and the cleavage of peroxide bond in PMS by UV irradiation and ultrasound can generate
71 $\text{SO}_4^{\cdot-}$ and $\cdot\text{OH}$ (Ghanbari and Moradi, 2017).

72 It has been recently reported that organic contaminants (e.g., carbamazepine,
73 sulfamethoxazole, chlorophenol) can be decomposed by direct PMS oxidation (i.e., no radical
74 initiator). Quenching studies and electron paramagnetic resonance spectrometry analysis
75 confirmed that contaminant transformation was attributed to the direct oxidation by PMS
76 without the contribution of radicals (Yang et al., 2018). However, little is known about the

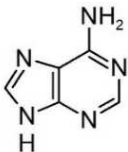
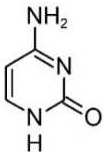
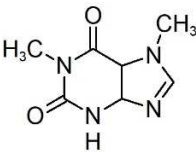
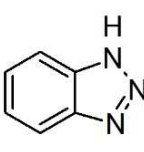
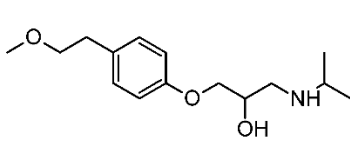
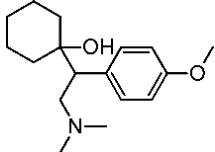
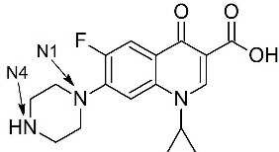
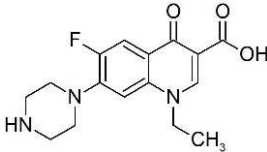
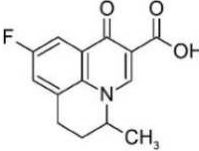
77 reaction mechanism of this non-radical process. Previous studies have reported that sulfur-
78 containing compounds (thioether sulfur of β -lactam antibiotics) can be substituted by the
79 oxygen from PMS to produce sulfoxide products (Chen et al., 2018). However, the oxygen
80 substitution pathway can be affected by steric hindrance, especially for contaminants with
81 complex structures (Chen et al., 2018).

82 PMS is a strong electron-acceptor with redox potential (E^0 ($\text{HSO}_5^-/\text{HSO}_4^{2-}$) = 1.82 V_{NHE})
83 (Steele and Appelman, 1982). Because of its strong electrophilic character, PMS can
84 oxidise/degrade contaminants by electron-withdrawing with carbon nanotube as electron-
85 transfer mediator (Yun et al., 2017). It has been reported that PMS can rapidly inactivate the
86 disease-associated prion protein. In this process, the amino acid residues of prion protein
87 were oxidised by PMS through the formation of methionine sulfone and hydroxylated
88 tryptophan residues (Chesney et al., 2016). The transformation of methionine sulfoxide to
89 methionine sulfone might be explained by the oxygen transfer mechanism mentioned above.
90 However, the formation of hydroxylated tryptophan residues suggested that there might be
91 other reaction pathways for the PMS non-radical process, especially for nitrogenous
92 compounds.

93 In this study, the reactivity of PMS with various nitrogen-containing compounds was
94 investigated, including nitrogenous heterocyclic compounds, aliphatic amines, and
95 fluoroquinolones (Table 1). Degradation kinetics experiments (i.e., involving the effect of pH,
96 and common water matrix components) were conducted on the selected fluoroquinolones due
97 to their high reactivity with PMS. Fluoroquinolones are among the most consumed antibiotic
98 classes in the world. Due to their resistance to biodegradation and high adsorption affinity,
99 fluoroquinolones show long half-life times in the environment (e.g., 10.6 days in surface
100 water and 580 days in soil). Fluoroquinolones have been detected in wastewater, surface
101 water, groundwater and sediment/soil at concentrations ranging from ng/L to mg/L (Van

102 Doorslaer et al., 2014). As shown in Table 1, fluoroquinolones are characterized by a core
103 quinolone ring structure containing a nitrogen atom. Ciprofloxacin, norfloxacin, and
104 enrofloxacin also have a piperazine ring with two more amine nitrogen atoms. The
105 transformation products of ciprofloxacin and enrofloxacin after PMS exposure were
106 tentatively identified by high-resolution mass spectrometry. MS² and MS³ fragmentation were
107 applied for most compounds for structural identification. Based on the characteristics of the
108 transformation products, possible reaction mechanisms of PMS reaction with nitrogenous
109 compounds were proposed. Agar diffusion tests were applied to investigate the residual
110 antibacterial activity of ciprofloxacin after PMS oxidation.

111 Table 1. Compounds investigated in this study

Adenine	Cytosine	Caffeine	Benzotriazole
			
Metoprolol	Venlafaxine	Ciprofloxacin (CIP) $pK_a=6.2, 8.8^a$	Norfloxacin
			
Enrofloxacin (ENR) $pK_a=6.1, 7.7^a$	Flumequine	1-(2-fluorophenyl) piperazine	
			
^a pK_a values were obtained from Jiang et al. (2016)			

112

113 **2. Materials and methods**

114 **2.1 Chemical Reagents**

115 All chemicals were of analytical grade or higher and used as received without further
116 purification. Potassium peroxymonosulfate (available as Oxone[®]), adenine ($\geq 99\%$),
117 cytosine ($\geq 99\%$), caffeine ($> 99\%$), benzotriazole (99%), ciprofloxacin ($\geq 98\%$), norfloxacin
118 ($\geq 98\%$), enrofloxacin ($\geq 98\%$), flumequine ($\geq 97\%$), 1-(2-fluorophenyl) piperazine (97%),
119 metoprolol ($\geq 98.5\%$), venlafaxine ($\geq 98\%$), *tert*-butanol ($\geq 99\%$), and ethanol (pure) were
120 purchased from Sigma-Aldrich. The Suwannee River hydrophobic acid fraction was
121 previously isolated (Croué et al., 2000) and used to study the effect of natural organic
122 matter (NOM) on the degradation rate of ciprofloxacin by PMS. All solutions were prepared
123 in ultrapure water (18.2 M Ω cm, Milli-Q, Purelab Classic).

124 **2.2 Experimental Procedures**

125 Experiments were conducted in amber glass bottles at room temperature ($22 \pm 1^\circ\text{C}$).
126 Predetermined volumes of target compounds and PMS stock solutions were injected into 25
127 mL of 10 mM phosphate (pH = 6.2–8) or borate (pH = 8.2–11) buffer to obtain the desired
128 initial concentrations. Samples were periodically collected and quenched with excess
129 sodium thiosulfate. For most experiments, the initial concentrations used for target
130 compound and PMS were 5 and 100 μM , respectively. To better identify the transformation
131 products, high concentrations of ciprofloxacin and enrofloxacin (50 μM) were treated with
132 50 μM and 1 mM of PMS. The influence of dissolved oxygen on the formation of
133 transformation products from enrofloxacin was investigated by purging the solution (before
134 PMS spiking) with N₂ until the dissolved oxygen concentration was reduced to 0.21 mg/L.
135 The solution was kept in N₂-purging throughout the experiment (20 min). The concentration
136 of dissolved oxygen was measured using a WTW Oxi 330 Oxygen meter. For antibacterial

137 activity tests, 5 μM of ciprofloxacin was degraded by 100 and 250 μM PMS. Most
138 experiments were conducted at least in duplicate.

139 **2.3 Analytical Methods**

140 A quantitative analysis of target compounds was conducted with a High-Performance
141 Liquid Chromatography (HPLC, Agilent 1100) coupled with a Diode Array Detector (DAD,
142 Agilent 1100) and an XDB-C18 column (5 μm , 4.6 \times 150 mm, Agilent). Mobile phase
143 composition followed various isocratic mixtures of methanol or acetonitrile with 10 mM
144 phosphate buffer. All compounds were analysed at their maximum UV absorption. Detailed
145 information on HPLC methods is provided in the supporting information section (Table S1).
146 The concentration of the residual PMS was determined according to an ABTS colorimetric
147 method previously published (Zhang et al., 2016). Briefly, 1 mL of sample was spiked into
148 a mixed solution of 0.5 mL of ABTS (20 mM) and 0.2 mL of CoSO_4 (20 mM), then allowed
149 to react for 1 min where a green-colored ABTS radical was formed. Then, 10 mL of H_2SO_4
150 (2%) was immediately added, followed by the spectrometric measurement at 734 nm (Cary
151 60, Agilent). The transformation products of ciprofloxacin and enrofloxacin were identified
152 using an Accela 600 Liquid Chromatography system coupled to a High-Resolution Mass
153 Spectrometry (LC-HRMS, LTQ Orbitrap XL, Thermo Fisher), and fitted with an
154 Electrospray Ion Source (ESI). Compounds were separated on a kinetex C18 column (2.6
155 μm , 100 \times 2.1 mm, Phenomenex). Full scan and MS^2 fragmentation scans were acquired in
156 positive ionisation mode (+eV). MS^3 fragmentation was additionally applied for compounds
157 with major peak areas on LC-HRMS. Details on LC-HRMS parameters are provided in
158 Table S2.

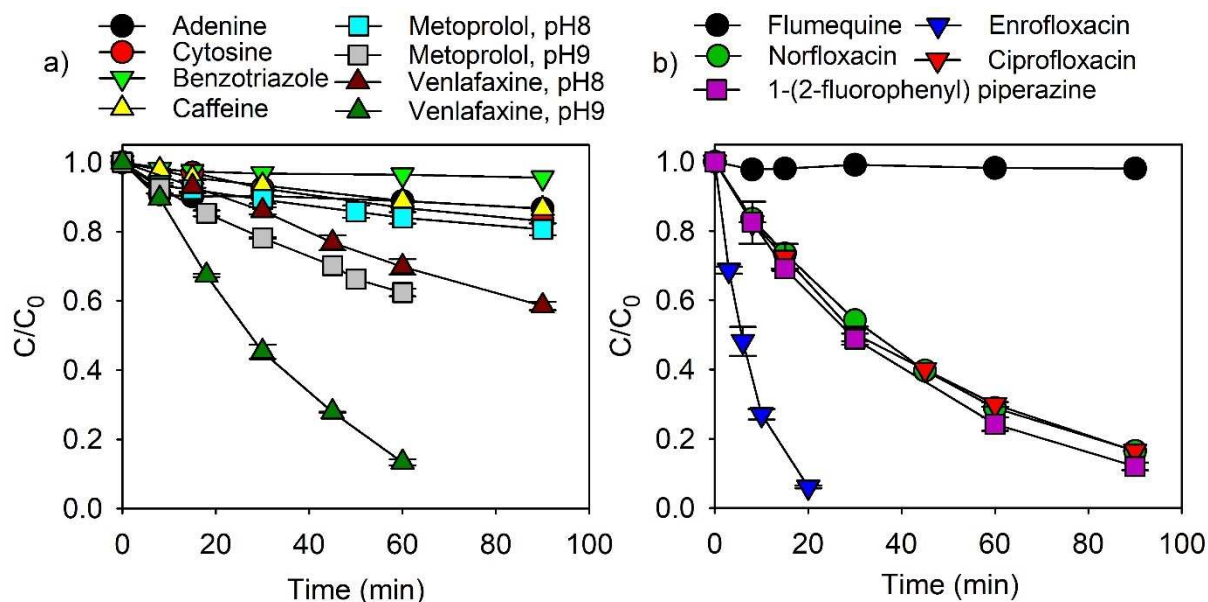
159 The distribution coefficients ($\log D$) of compounds were calculated on a public Web source
160 developed by ChemAxon (<https://chemicalize.com>, accessed in July 2019).

161 **2.4 Antibacterial Activity Test**

162 Agar disk-diffusion tests were conducted to investigate the antibacterial activity of
163 ciprofloxacin (5 μM) after PMS exposure (100 and 250 μM) using *Escherichia. coli* B (*E.*
164 *coli* B) as the test microorganism according to the Clinical and Laboratory Standards
165 Institute (CLSI, 2012). Briefly, lysogeny (LB) agar plates were inoculated with 100 μL of
166 an overnight culture of *E. coli* B, equivalent to 0.5 McFarland. Then, blank antibiotic
167 cartridges (approximately 6 mm in diameter) containing the test solutions, were placed on
168 the agar surface. The diameters of inhibition zones around discs were measured after the
169 plate was incubated overnight at 37°C. A wider zone of no growth indicates a stronger
170 antibacterial activity of the test solution. The removal of ciprofloxacin antibacterial activity
171 after PMS exposure was determined by comparing the diameters of the inhibition zones
172 from PMS-treated samples of ciprofloxacin and the ciprofloxacin standards with known
173 concentrations (0.2, 0.5, 1, 2, 3, 4, and 5 μM). Each sample was tested in triplicates.

174 **3. Results and Discussion**

175 **3.1 Reactivity of PMS with various nitrogen containing compounds**



176

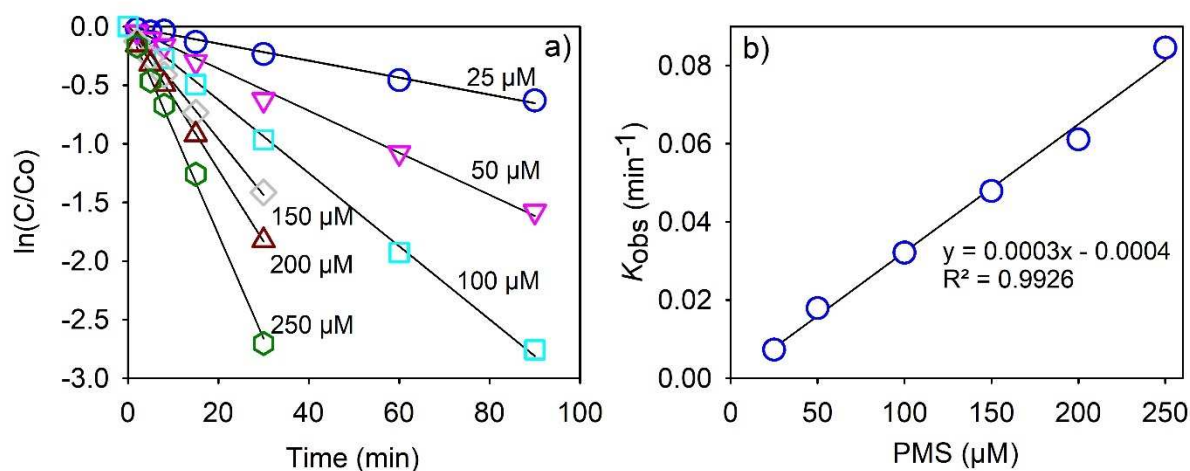
177 **Figure 1.** Relative removal of the selected nitrogenous compounds by PMS (Target
178 compound: 5 μ M; PMS: 100 μ M; 10 mM phosphate buffer at pH 8; Metoprolol and
179 venlafaxine were also tested in 10 mM borate buffer at pH 9)

180 The degradation of the selected nitrogenous compounds by PMS was individually studied in
181 the absence of chemical catalysts or UV irradiation. Less than 20% of the selected
182 nitrogenous heterocyclic compounds (i.e., adenine, cytosine, benzotriazole, and caffeine)
183 were removed at pH 8 within 90 min (Figure 1a). Approximately 40% of venlafaxine
184 (aliphatic tertiary amine) was eliminated at pH 8 for the same time frame, which was faster
185 than metoprolol (aliphatic secondary amine). The degradation of metoprolol and venlafaxine
186 by PMS was influenced by pH, suggesting that the amine group was likely the main reaction
187 site. The degradation rates were faster at pH 9 than at pH 8 for both compounds, possibly due
188 to the higher proportion of deprotonated molecules at higher pH. Venlafaxine was degraded

189 faster than metoprolol in both conditions, revealing that PMS might be more reactive with
190 tertiary amines than secondary amines.

191 The degradation efficiencies of fluoroquinolones and their related compounds significantly
192 varied depending on their structural characteristics (Figure 1b). Flumequine, a
193 fluoroquinolone without a piperazine ring (Table 1), was stable in the presence of PMS in
194 these experimental conditions, suggesting that PMS does not react with quinolone rings. The
195 cyclopropane ring of ciprofloxacin (CIP) is substituted by an ethyl group in norfloxacin. 1-(2-
196 fluorophenyl) piperazine has a fluorobenzene ring instead of the quinolone ring. However,
197 CIP, norfloxacin, and 1-(2-fluorophenyl) piperazine have the same piperazine ring structure
198 and exhibited comparable degradation rates toward PMS (80% removal within 90 min).
199 These results indicated that the piperazine ring was the main reaction site for PMS. This was
200 further supported by LC-HRMS analyses (section 3.4) from which only piperazine ring
201 cleavage products were identified after PMS exposure. The N4 (CIP in Table 1 for atom
202 numbering) in the piperazine ring of enrofloxacin (ENR) is substituted by an ethyl group
203 (tertiary amine), which differs from CIP (secondary amine). ENR was degraded considerably
204 faster than CIP, a result that was consistent with the above evidence that tertiary amines were
205 more susceptible to PMS attack than secondary amines. Overall results suggested that PMS
206 was more reactive towards fluoroquinolones (except for flumequine) than the selected
207 nitrogenous heterocyclic compounds and aliphatic amines at pH 8. More detailed experiments
208 were conducted on CIP and ENR to study the reaction mechanism of PMS with nitrogenous
209 compounds.

210 **3.2 Degradation kinetics of fluoroquinolones by PMS**



211

212 **Figure 2.** a) Effect of the initial concentration of PMS on ciprofloxacin degradation; b) k_{obs}

213 versus initial concentration of PMS (Ciprofloxacin: 5 μM ; 10 mM borate buffer at pH 8.2)

214 The presence of excess ethanol, *t*-BuOH, and NaN_3 did not affect the degradation kinetic of

215 CIP (Figure S1), which confirmed previous findings that no $\text{SO}_4^{\bullet-}$, $\bullet\text{OH}$, and $^1\text{O}_2$ were

216 involved during the oxidation of fluoroquinolones by PMS (Zhou et al., 2018). The

217 degradation of CIP was promoted by increasing the initial PMS dose (25–250 μM), following

218 pseudo-first order kinetics ($R^2 > 0.99$) (Figure 2a). The measured rate constants, k_{obs} , were

219 derived from the slope of $\ln(C/C_0)$ versus time. As shown in Figure 2b, k_{obs} exhibited a

220 linear relationship toward the initial PMS dose, suggesting that the overall reaction rate can

221 be described by the second-order kinetic. According to equation 1 and 2, the apparent second-

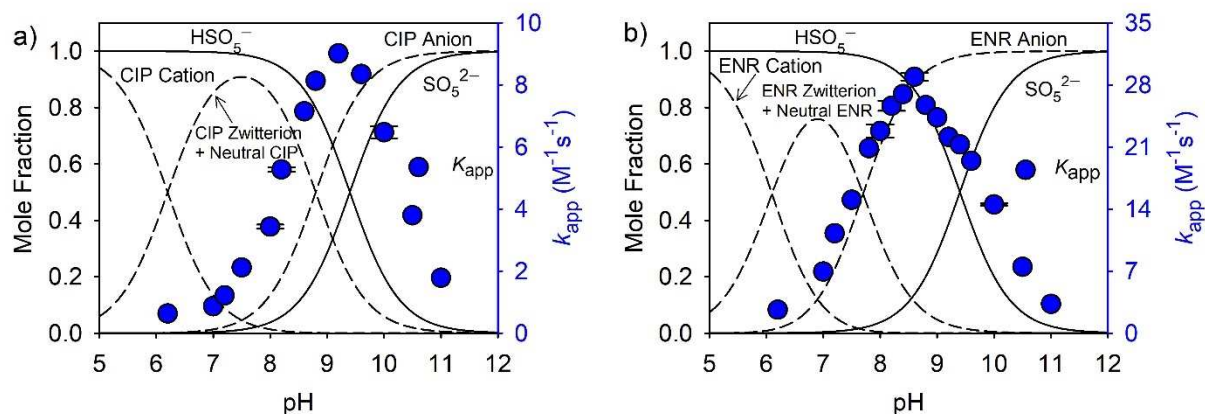
222 order rate constant, k_{app} , of CIP with PMS was calculated as 5.28 ± 0.08 ($\text{M}^{-1} \text{s}^{-1}$) at pH 8.2,

223 which was comparable with previously reported results by Zhou et al. (2018) ($\sim 6 \text{ M}^{-1} \text{s}^{-1}$ at

224 pH 8).

225
$$\frac{d[CIP]}{dt} = -k_{obs}[CIP] \quad (1)$$

226
$$\frac{d[CIP]}{dt} = -k_{app}[CIP][PMS] \quad (2)$$



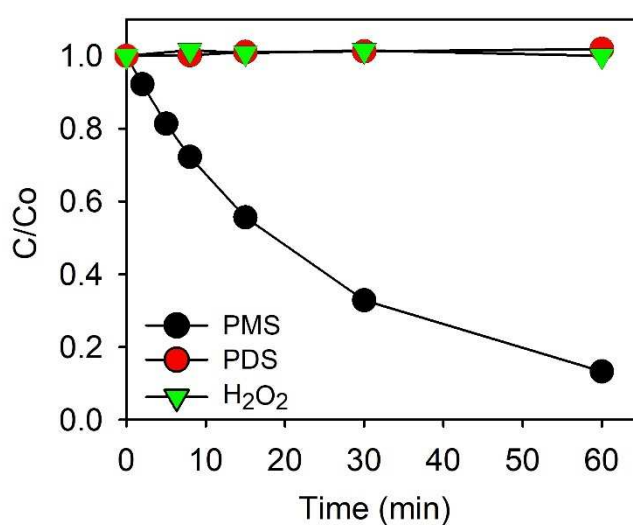
227

228 **Figure 3.** The effect of pH on the distribution of acid-base species of ciprofloxacin (a) and
 229 enrofloxacin (b), and their apparent second-order constants with PMS. (CIP or ENR: 5 μ M;
 230 PMS: 100 μ M; 10 mM phosphate or borate buffer at pH 6.2–11; The acid-base species of
 231 ciprofloxacin were shown in Scheme S1 as an example)

232 As illustrated in Figure 3, the degradation efficiency (k_{app}) of CIP and ENR by PMS were
 233 highly pH-dependent. The pH-dependent reactivity of fluoroquinolones was also observed
 234 with free chlorine (Dodd et al., 2005), manganese oxide (Zhang and Huang, 2005), ozone
 235 (Dodd et al., 2006), and chlorine dioxide (Wang et al., 2010). The pH-dependence of
 236 fluoroquinolones degradation can be explained by the change in the distribution of
 237 fluoroquinolones and PMS acid-base species with pH (Zhou et al., 2018). The pK_a values of
 238 CIP and ENR relevant to these experimental conditions were provided in Table 1. pK_{a1} and
 239 pK_{a2} were related to the deprotonation of the carboxylic group and the protonation of N4 in
 240 the piperazine ring, respectively (Scheme S1) (Takács-Novák et al., 1990). PMS dissociated
 241 into SO_5^{2-} at alkaline pH ($HSO_5^- + H_2O \rightleftharpoons SO_5^{2-} + H_3O^+$, $pK_{a2}=9.4$) (Ball and Edwards,
 242 1956). The k_{app} values of CIP and ENR increased with increasing molar fraction of the
 243 anionic species (Figure 3), suggesting that the anion forms of CIP and ENR were most
 244 susceptible to PMS oxidation. In general, N4 in piperazine ring is deprotonated when CIP and
 245 ENR are present in anionic form, consequently showing a stronger nucleophilic character.

246 The highest k_{app} values of CIP and ENR were found at around pH 9 and pH 8.6, respectively;
247 then, it sharply decreased with increasing relative abundance of SO_5^{2-} , suggesting that SO_5^{2-}
248 is a weaker oxidant compared to PMS. SO_5^{2-} was also reported as less reactive than PMS
249 with β -lactam antibiotics, due to its weaker electrophilic property (Chen et al., 2018). Notably,
250 PMS showed higher reactivity towards ENR than CIP in all studied pH conditions.

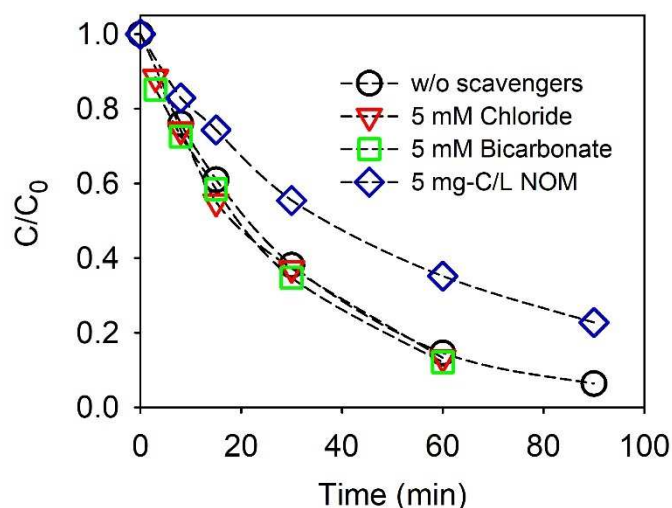
251 3.3 Comparison with other peroxides and the effect of the water matrix



252

253 **Figure 4.** Relative removal of ciprofloxacin by PMS, PDS, and H₂O₂ (Ciprofloxacin=5 μM ;
254 Oxidants=100 μM ; 10 mM phosphate buffer at pH 8)

255 The reactivity of PMS was compared with other peroxides. Unlike PMS, PDS and H₂O₂ did
256 not react with CIP under the same experimental conditions (Figure 4). These results
257 suggested that PDS and H₂O₂, as symmetric peroxides, tend to be more stable; whereas, PMS
258 is a more efficient electron acceptor, possibly due to its asymmetric structure (Lei et al.,
259 2016). This is consistent with previous findings indicating that PMS was more efficient
260 compared to PDS for the removal of organic contaminants during the mediated electron
261 transfer through carbon nanotubes (Yun et al., 2017; Yun et al., 2018).



262

263 **Figure 5.** Effect of the water matrix on the degradation of ciprofloxacin by PMS

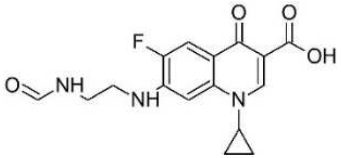
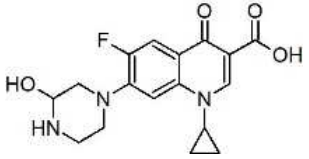
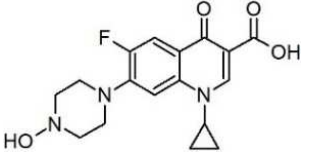
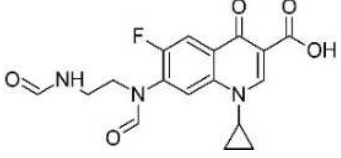
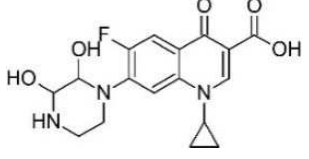
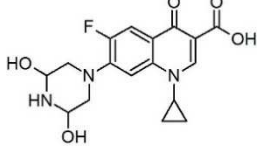
264 (Ciprofloxacin: 5 μ M; PMS: 100 μ M; Chloride= Bicarbonate: 5 mM; NOM: 5 mg-C/L; 10
 265 mM borate buffer at pH 8.2)

266 The water matrix components can compete with the target contaminants to consume radicals
 267 during AOPs, consequently lowering the treatment efficiency. The effect of the common
 268 water matrix components (i.e., NOM, chloride, and bicarbonate ions) on the degradation of
 269 CIP by PMS was investigated. Unlike the radical-based AOPs, the degradation of CIP by
 270 PMS was not impacted by the presence of 5 mM of chloride and bicarbonate ions (Figure 5).
 271 PMS was previously reported to oxidize chloride ion into chlorine, which can contribute to
 272 contaminant degradation (Fortnum et al., 1960). However, the acceleration of the CIP
 273 degradation rate was not observed in this study upon the addition of 5 mM of chloride. This
 274 can be explained by the insufficient formation of chlorine due to the low reaction rate
 275 constant of chloride with PMS ($1.4 \times 10^{-3} \text{ M}^{-1} \text{ s}^{-1}$) (Fortnum et al., 1960), which was about
 276 three orders of magnitude lower than the k_{app} of CIP with PMS in this study ($5.28 \pm 0.08 \text{ M}^{-1}$
 277 s^{-1} at pH 8.2). The addition of 5 mg-C/L NOM slightly inhibited the removal of CIP,
 278 suggesting that PMS can react with NOM.

279 **3.4 Transformation products**280 **Table 2.** Transformation products of ciprofloxacin (CIP) detected by LC-HRMS

Compound	RT ^a	Molecular formula	Molecular mass ^b	MS ² ^c , <i>m/z</i>	Proposed structures
CIP	12.6	C ₁₇ H ₁₉ O ₃ N ₃ F	332.1404 (-0.169)	314, 288	
P263	16.7	C ₁₃ H ₁₂ O ₃ N ₂ F	263.0826 (-0.369)	245, 263	
P291	17.4	C ₁₄ H ₁₂ O ₄ N ₂ F	291.0775 (-0.177)	273, 291	
P306	12.3	C ₁₅ H ₁₇ O ₃ N ₃ F	306.1248 (-0.183)	306, 288	
P320	18.0	C ₁₅ H ₁₅ O ₄ N ₃ F	320.1034 (-0.252)	302, 320 MS ³ : 258, 265, 285, 302, 224, 245, 217	
P334a	11.1	C ₁₆ H ₁₇ O ₄ N ₃ F	334.1198 (-0.750)	316, 317, 314, 306, 296 MS ³ : 296, 245,	

230, 271, 288

P334b	17.3	C ₁₆ H ₁₇ O ₄ N ₃ F	334.1199 (-0.301)	316 MS ³ : 271, 289, 298, 245	
P348a	8.2	C ₁₇ H ₁₉ O ₄ N ₃ F	348.1348 (-1.841)	331, 287, 304 MS ³ : 287, 273	
P348b	17.3	C ₁₇ H ₁₉ O ₄ N ₃ F	348.1354 (-0.002)	330, 287 MS ³ : 285, 272, 310, 282	
P362	13.2	C ₁₇ H ₁₇ O ₅ N ₃ F	362.1143 (-0.985)	344, 362	
P364a	12.4	C ₁₇ H ₁₉ O ₅ N ₃ F	364.1302 (-0.372)	346, 364 MS ³ : 326, 288, 271	
P364b	16.5	C ₁₇ H ₁₉ O ₅ N ₃ F	364.1239 (-0.372)	346, 364, 328 MS ³ : 346, 328, 275, 257	

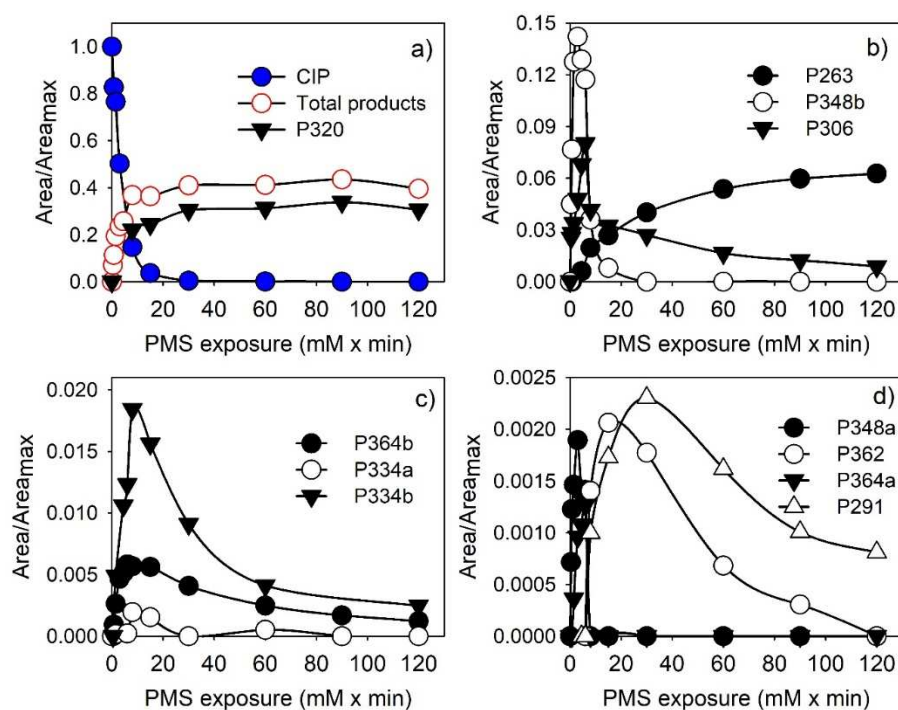
^a Retention time (min); ^b Experimental mass for [M+H]⁺; numbers in brackets represent the difference with the theoretical mass of the proposed compound (ppm); ^c MS³ fragmentation was additionally applied for P320, P334 (a, b), P348 (a, b) and P364 (a, b). The MS²/MS³ spectra of compounds were provided in the supporting

information (Figure S2-S13).

281 Eleven transformation products of CIP after PMS oxidation were detected by LC-HRMS
282 (Table 2). Their structures were tentatively proposed based on the accurate mass derived from
283 HRMS and MS²/MS³ fragmentation patterns (Figure S2-S13). The proposed structures
284 indicated that the degradation of CIP occurred by the hydroxylation and dealkylation of the
285 piperazine ring, with the subsequent formation of aldehyde and amide moieties. The core
286 quinolone ring of CIP remained intact and no defluorination or decarboxylation products
287 were detected, which were the known transformation products of CIP during Fenton
288 oxidation (Giri and Golder, 2014), SO₄^{•-} (Jiang et al., 2016) and photolytic reactions (Paul et
289 al., 2010). These results were consistent with the fact that flumequine, which does not
290 incorporate a piperazine ring, did not react with PMS (Figure 1b). Several transformation
291 products (e.g., P263, P291, P306, P334, P348, P362, and P364) were also obtained during the
292 oxidative transformation of CIP by manganese oxide (Zhang and Huang, 2005), chlorine
293 dioxide (Wang et al., 2010), permanganate (Hu et al., 2011), and Ferrate (VI) (Yang et al.,
294 2016a), revealing that PMS may share a similar reaction mechanism with these oxidants.
295 However, structural isomers corresponding to CIP with one additional oxygen atom (P348a
296 and P348b) or two additional oxygen atoms (P364a and P364b) were detected in this study.
297 Particularly, P348a and P348b shared the same molecular weight, but different MS²/MS³
298 spectra (Figure S9 and S10, respectively) and retention time. P348a was proposed as a
299 hydroxylated analogue of CIP, with a hydroxyl group located on α -carbon; whereas, P348b
300 was a hydroxylamine compound. This may be further supported by the calculated distribution
301 coefficient ($\log D$) at pH 2.3 (pH of LC-HRMS mobile phase). P348b had a higher $\log D$ (1.15)
302 than P348a (-2.05), consequently showing a longer retention time on the reverse phase
303 column. P348b was believed to be rearranged from its *N*-oxide analogue, which is a known
304 mechanism for primary and secondary amines (Hübner et al., 2015). Most transformation

305 products (except for P263, P306, and P348) were not reported in a previous study on the
306 oxidation of 20 μM CIP by 0.1 mM PMS (Zhou et al., 2018), likely because higher CIP (50
307 μM) was applied in the current study to maximize the formation of by-products. Moreover,
308 the HRMS signal intensity of most products (e.g., P320, P334, P291) reached their maximum
309 when the PMS exposure was above 8 (mM \times min) (Figure 6), which was achieved by initially
310 applying 1 mM PMS in this study.

311 To the best of our knowledge, the transformation product P320 has only been reported from
312 the ozonation of CIP (Liu et al., 2012). The MS³ spectrum (Figure S6b) of P320 exhibited a
313 dominant ion cluster m/z 258 corresponding to the loss of an amide group ($-\text{CH}_2\text{ON}$) from
314 the major ion cluster m/z 302 in its MS² spectrum (Figure S6a). Thus, the postulated structure
315 of P320 is an amide moiety formed at the secondary aliphatic amine (N4) of the piperazine
316 ring.



317

318 **Figure 6.** The evolution of the normalized chromatographic peak areas of ciprofloxacin (CIP)

319 and its transformation products with PMS exposure. Area_{max} represents the peak area of

320 ciprofloxacin at t=0 (Ciprofloxacin: 50 μ M; PMS: 0.05 and 1 mM; 10 mM borate buffer at
321 pH 8.2)

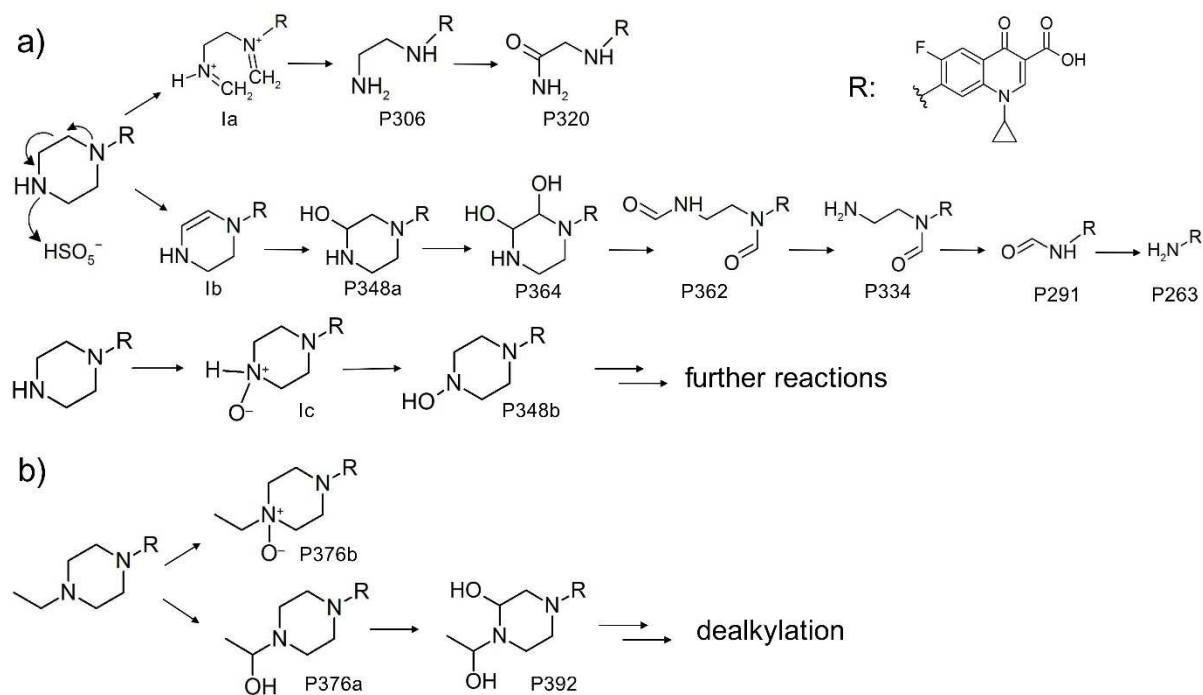
322 Figure 6 presents the evolution of the normalized chromatographic peak areas of CIP and its
323 transformation products with PMS exposure. P320 exerted the largest peak area among all
324 identified transformation products (i.e., close to the sum of the peak areas of all
325 transformation products). P320 was rapidly formed with the degradation of CIP and reached a
326 plateau. P263, which refers to the complete loss of the piperazine ring, gradually increased
327 with exposure time. Thus, P320 and P263 were the final products in these experimental
328 conditions, while all other compounds were intermediates showing a maximum production at
329 different oxidant exposures. For example, P334b and P362 reached their highest peak areas at
330 8 and 15 (mM \times min), respectively, while P320 almost reached a plateau, indicating that
331 P334b and P362 were unlikely the intermediates of P320.

332 Hydroxylated products (P376 and P392) were the major by-products after PMS oxidation of
333 ENR (Table S3), which was in accordance with a previous study (Zhou et al., 2018). Like
334 CIP, two structural isomers of ENR with an additional oxygen atom (i.e., P376a and P376b)
335 were identified. P376a was proposed as a hydroxylated ENR on α -carbon, while P376b was a
336 *N*-oxide analogue of ENR, although further confirmation with analytical standards is needed.
337 The log*D* value of P376b at pH 2.3 (1.09) was considerably higher than ENR (-1.19) and
338 P376a (-1.65), consistent with its longer retention time on the LC-HRMS chromatogram
339 (Table S3). Previous investigations have demonstrated that *N*-oxide analogues of tertiary
340 amines have higher retention times than their precursors on reverse-phase columns (Merel et
341 al., 2017). A transformation product of ENR after PMS oxidation was detected on the HPLC-
342 UV chromatogram (Figure S14), which was eluted after the ENR peak and proposed as
343 P376b based on an assumption that the eluting order of compounds was comparable on LC-
344 HRMS and HPLC-UV coupled with similar reverse-phase C18 columns. The HPLC-UV

345 peak area of P376b did not change during the experiments conducted with and without N₂-
 346 purged solutions (Figure S15). These results suggested that the dissolved oxygen did not
 347 contribute to the formation of ENR *N*-oxide. Alternatively, the oxygen likely originated from
 348 PMS itself. The *N*-oxide formation was also proposed for ENR oxidized by ozone (Dodd et
 349 al., 2006), manganese oxide (Zhang and Huang, 2005), and permanganate (Xu et al., 2016).

350 3.5 Proposed reaction mechanisms

351 **Scheme 1.** Proposed degradation mechanisms of ciprofloxacin (a) and enrofloxacin (b) by
 352 PMS (Ia, Ib, and Ic are the proposed intermediates)



354 In accordance with the postulated structures of the transformation products and the evolution
 355 of their peak areas on LC-HRMS chromatograms, reaction mechanisms for the oxidative
 356 transformation of CIP by PMS were proposed (Scheme 1a). The reaction was initiated by the
 357 direct electron transfer from the piperazine ring to PMS. In this process, PMS acted as an
 358 electron acceptor, rather than a radical precursor, to directly oxidize CIP. The N4 atom of
 359 piperazine ring was the critical site for the electrophilic attack of PMS. The N1 atom is

360 known as less reactive to electrophiles than N4 due to its direct connection to the
361 fluoroquinolone ring substituted by strong electron-withdrawing fluorine and –COOH (Dodd
362 et al., 2005; Giri and Golder, 2014). Nevertheless, previous studies have demonstrated that
363 the piperazine ring should be considered as a whole reaction centre with the contribution of
364 both nitrogen atoms to electron-transfer (Wang et al., 2010). This could explain the higher
365 reactivity of PMS with piperazine ring-containing compounds, compared to aliphatic amines
366 (metoprolol and venlafaxine), as shown in Figure 1.

367 The initial electron transfer from the piperazine ring to PMS produces an imine intermediate
368 (Ia, Scheme 1a) as proposed by Dodd et al. (2005) and Wang et al. (2010) for the oxidation of
369 CIP by free chlorine and chlorine dioxide, respectively. The hydrolysis of the imine
370 intermediate rapidly induced the dealkylation of the piperazine ring to generate P306. The
371 subsequent electron transfer from the amine group of P306 to PMS was followed by
372 hydrolysis producing P320. The presence of highly electron-withdrawing carbonyl group
373 (C=O) in P320 possibly limited the electron transfer from amide-N to PMS. Thus, P320 was
374 stable in the presence of excess PMS (Figure 6a). The formation of hydroxylated products
375 P348a and P364 suggested the presence of a similar enamine intermediate (Ib, Scheme 1a),
376 which has been proposed for the reactions of permanganate (Hu et al., 2011) and Ferrate (IV)
377 (Yang et al., 2016a) with CIP. The double bond of enamine can be oxidized to aldehyde
378 moieties (P362, P334, and P291), leading to the complete degradation of piperazine ring.

379 The oxygen transfer from PMS to secondary amine CIP generates *N*-oxide intermediate (Ic,
380 Scheme 1a), which subsequently rearranged to hydroxylamine compound (P348b) (Lee and
381 von Gunten, 2016). As shown in Figure 6b, the intensity of P348b reached the maximum at 3
382 mM (mM × min) and rapidly decreased with PMS exposure, suggesting that P348b was
383 subjected to further reactions in the presence of excess PMS. The oxygen transfer pathway
384 might involve the transfer of the distal oxygen in the peroxide bond of PMS to CIP. An

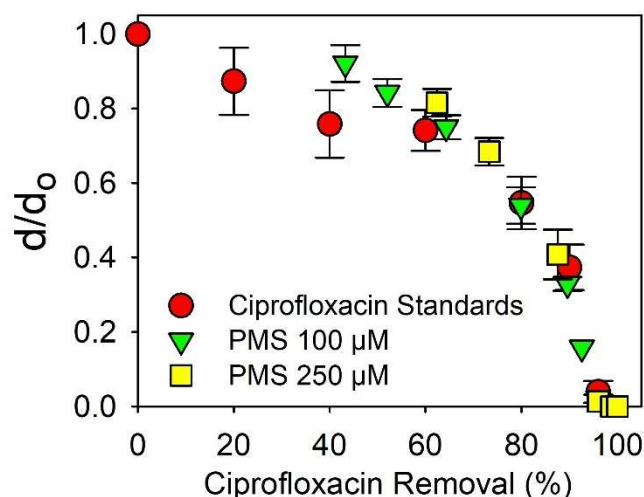
385 oxygen transfer mechanism was also proposed for the oxidation of arsenite As (III) to As (V)
386 by PMS (Wang et al., 2014). The thioether sulfur of β -lactam antibiotics can be substituted
387 by the oxygen from PMS to produce sulfoxide products (Chen et al., 2018). The aniline
388 moieties of sulfonamide antibiotics can be converted to nitroso or nitrobenzene moieties
389 through PMS oxygen substitution (Yin et al., 2018).

390 PMS was also proposed to react with tertiary amine ENR via oxygen transfer to generate
391 ENR *N*-oxide, P376b (Scheme 1b). The direct electron transfer pathway also occurred during
392 PMS oxidation of ENR and led to the hydroxylation on α -carbon to produce P376a and P392.
393 Based on the degradation pathway of CIP, it was postulated that the hydroxylated products
394 P392 might undergo further oxidation, followed by the dealkylation of the piperazine ring.

395 Additional investigation is needed to confirm the major pathway of PMS reaction (electron
396 transfer *vs* oxygen transfer) with nitrogenous compounds, which might be helpful to explain
397 the different reaction potential of PMS towards secondary and tertiary amine moieties as
398 mentioned above.

399 **3.6 Antibacterial activity assays**

400 Fluoroquinolones inhibit the bacterial DNA replication by hydrogen binding and charge
401 interactions with the relaxed DNA. The core quinolone structure would be responsible for
402 DNA-binding (Dodd et al., 2006), while the fluorine substitute plays an important role in
403 inhibiting the DNA gyrase and enhancing cell permeation (Serna-Galvis et al., 2017).



404

405 **Figure 7.** Antibacterial activity removal of ciprofloxacin (CIP) during PMS treatment. d_0
 406 represents the diameter of the inhibition zone in agar plate formed by 5 μM of CIP standard
 407 solution (CIP standards: 0.2, 0.5, 1, 2, 3, 4 and 5 μM ; for PMS treatment, initial concentration
 408 of CIP:5 μM , PMS: 100 and 250 μM , 10 mM borate buffer at pH 8.2)

409 Based on LC-HRMS results, the transformation products of CIP after PMS treatment still
 410 retained the core quinolone structure, raising concerns about the residual antibacterial activity.
 411 Thus, agar diffusion assays were conducted with *E. coli B* as an indicator. As shown in
 412 Figure 7, the antibacterial activity of the solution gradually reduced with the removal of CIP
 413 during PMS treatment. However, after 40 to 50% removal of CIP with 100 μM of PMS, the
 414 sample resulted in a larger inhibition zone in the agar plate than CIP standard solutions. This
 415 result indicated that the transformation products at an earlier stage (e.g., hydroxylamine
 416 product P348b, Figure 6b) might still exert antibacterial potency. The residual antibacterial
 417 activity was efficiently removed with the complete degradation of CIP, suggesting that the
 418 major final products P320 and P263 showed negligible antibacterial activity compared to CIP.
 419 The structural modifications on the piperazine ring alter the acid-base speciation and
 420 significantly affect fluoroquinolones cell permeation (Paul et al., 2010). Although the amide
 421 and aldehyde moieties produced after PMS exposure kept the core quinolone structure in this

422 study, their physicochemical characteristics might be significantly different from those of CIP,
423 consequently reducing their uptake by bacteria cell and binding to DNA. The current results
424 were in agreement with previous findings reporting that the photolytic transformation
425 products of CIP retaining the quinolone ring significantly diminished the antibacterial
426 potency of the parent antibiotic (Paul et al., 2010).

427 **4. Conclusion**

- 428 • PMS can efficiently degrade the selected fluoroquinolones (except for flumequine),
429 followed by aliphatic amines and nitrogenous heterocyclic compounds. The common
430 water matrix components (e.g., bicarbonate and chloride ions) did not impact the
431 degradation rate of CIP by PMS. The electron transfer from the piperazine ring of CIP
432 to PMS induced the dealkylation and hydroxylation of the molecule and led to the
433 formation of amide and aldehyde moieties. PMS was also proposed to react with CIP
434 and ENR via oxygen transfer to produce hydroxylamine analogue of CIP and ENR *N*-
435 oxide, respectively.
- 436 • PMS efficiently removed the antibacterial activity of CIP. However, the
437 transformation products in earlier stages of the reaction still exerted antibacterial
438 potency. A complete elimination of the parent compound, as well as its transformation
439 products, is required during the fluoroquinolone treatment by PMS.

440 The findings of this study suggested that the direct PMS oxidation can be selectively applied
441 for the removal of nitrogenous compounds (e.g., fluoroquinolones). However, some
442 persistent transformation products (e.g., *N*-oxides) can be formed, which are inert to the
443 biodegradation (Hübner et al., 2015). Unlike radical-based processes, this treatment can
444 maintain its efficiency in complex water matrixes. However, NOM slightly inhibited the
445 degradation of CIP by PMS. Therefore, additional studies are needed to investigate the

446 reactivity of PMS with NOM fractions of different characteristics to optimize the PMS dose
447 for its best treatment efficiency. Because environmental components (e.g., nitrogen and
448 sulfur-containing organics) (Chen et al., 2018; Yang et al., 2018) are susceptible to react with
449 PMS, the non-radical pathway might hinder the formation of radicals during PMS-activated
450 AOPs, consequently limiting the removal of the targeted hazardous compounds. The electron
451 and oxygen transfer pathways proposed in this study assist in understanding the non-radical
452 reaction mechanism of PMS with organic contaminants and in predicting the formation of
453 potential transformation products. Similar mechanistic studies and screening of
454 transformation products can be extended to other oxidants used during water treatment,
455 which also have similar peroxide bond and asymmetric structure to PMS, such as organic
456 peracids (Luukkonen and Pehkonen, 2017).

457 **Acknowledgments**

458 Curtin University (Curtin International Postgraduate Research Scholarship) and Water
459 Research Australia (WaterRA Postgraduate Scholarship) are gratefully acknowledged for
460 providing financial support for M. Nihemaiti. The authors would like to thank Dr Francesco
461 Busetti and Dr Zuo Tong How for their support on LC-MS analysis, and Dr Leonardo
462 Gutierrez (Universidad del Pacifico) for proofreading.

463 **References**

- 464 Ball, D.L.Edwards, J.O., 1956. The Kinetics and Mechanism of the Decomposition of Caro's
465 Acid. I. *Journal of the American Chemical Society* 78(6), 1125-1129.
- 466 Chen, J., Fang, C., Xia, W., Huang, T.Huang, C.-H., 2018. Selective Transformation of β -
467 Lactam Antibiotics by Peroxymonosulfate: Reaction Kinetics and Nonradical
468 Mechanism. *Environmental Science & Technology* 52(3), 1461-1470.
- 469 Chesney, A.R., Booth, C.J., Lietz, C.B., Li, L.Pedersen, J.A., 2016. Peroxymonosulfate
470 Rapidly Inactivates the Disease-Associated Prion Protein. *Environmental Science &*
471 *Technology* 50(13), 7095-7105.
- 472 CLSI, 2012. Performance Standards for Antimicrobial Disk Susceptibility Tests. Approved
473 Standard, 7th ed. Clinical and Laboratory Standards Institute, Wayne, Pennsylvania,
474 USA.
- 475 Croué, J.-P., Korshin, G.V.Benjamin, M., 2000. Characterisation of Natural Organic Matter
476 in Drinking Water. American Water Works Association Research Foundation, Denver,
477 CO, USA.
- 478 Dodd, M.C., Buffle, M.-O.von Gunten, U., 2006. Oxidation of Antibacterial Molecules by
479 Aqueous Ozone: Moiety-Specific Reaction Kinetics and Application to Ozone-Based
480 Wastewater Treatment. *Environmental Science & Technology* 40(6), 1969-1977.
- 481 Dodd, M.C., Shah, A.D., von Gunten, U.Huang, C.-H., 2005. Interactions of Fluoroquinolone
482 Antibacterial Agents with Aqueous Chlorine: Reaction Kinetics, Mechanisms, and
483 Transformation Pathways. *Environmental Science & Technology* 39(18), 7065-7076.
- 484 Fortnum, D.H., Battaglia, C.J., Cohen, S.R.Edwards, J.O., 1960. The Kinetics of the
485 Oxidation of Halide Ions by Monosubstituted Peroxides. *Journal of the American*
486 *Chemical Society* 82(4), 778-782.
- 487 Ghanbari, F.Moradi, M., 2017. Application of peroxymonosulfate and its activation methods
488 for degradation of environmental organic pollutants: Review. *Chemical Engineering*
489 *Journal* 310, 41-62.
- 490 Giri, A.S.Golder, A.K., 2014. Ciprofloxacin degradation from aqueous solution by Fenton
491 oxidation: reaction kinetics and degradation mechanisms. *RSC Advances* 4(13), 6738-
492 6745.
- 493 Hu, L., Stemig, A.M., Wammer, K.H.Strathmann, T.J., 2011. Oxidation of Antibiotics during
494 Water Treatment with Potassium Permanganate: Reaction Pathways and Deactivation.
495 *Environmental Science & Technology* 45(8), 3635-3642.
- 496 Hübner, U., von Gunten, U.Jekel, M., 2015. Evaluation of the persistence of transformation
497 products from ozonation of trace organic compounds – A critical review. *Water*
498 *Research* 68, 150-170.
- 499 Ike, I.A., Linden, K.G., Orbell, J.D.Duke, M., 2018. Critical review of the science and
500 sustainability of persulphate advanced oxidation processes. *Chemical Engineering*
501 *Journal* 338, 651-669.
- 502 Jiang, C., Ji, Y., Shi, Y., Chen, J.Cai, T., 2016. Sulfate radical-based oxidation of
503 fluoroquinolone antibiotics: Kinetics, mechanisms and effects of natural water
504 matrices. *Water Research* 106, 507-517.
- 505 Lee, Y.von Gunten, U., 2016. Advances in predicting organic contaminant abatement during
506 ozonation of municipal wastewater effluent: reaction kinetics, transformation products,
507 and changes of biological effects. *Environmental Science: Water Research &*
508 *Technology* 2(3), 421-442.

- 509 Lei, Y., Chen, C.-S., Ai, J., Lin, H., Huang, Y.-H., Zhang, H., 2016. Selective decolorization
510 of cationic dyes by peroxymonosulfate: non-radical mechanism and effect of chloride.
511 RSC Advances 6(2), 866-871.
- 512 Liu, C., Nanaboina, V., Korshin, G.V., Jiang, W., 2012. Spectroscopic study of degradation
513 products of ciprofloxacin, norfloxacin and lomefloxacin formed in ozonated
514 wastewater. Water Research 46(16), 5235-5246.
- 515 Lutze, H.V., Bircher, S., Rapp, I., Kerlin, N., Bakkour, R., Geisler, M., von Sonntag,
516 C.Schmidt, T.C., 2015. Degradation of Chlorotriazine Pesticides by Sulfate Radicals
517 and the Influence of Organic Matter. Environmental Science & Technology 49(3),
518 1673-1680.
- 519 Luukkonen, T., Pehkonen, S.O., 2017. Peracids in water treatment: A critical review. Critical
520 Reviews in Environmental Science and Technology 47(1), 1-39.
- 521 Merel, S., Lege, S., Yanez Heras, J.E., Zwiener, C., 2017. Assessment of N-Oxide Formation
522 during Wastewater Ozonation. Environmental Science & Technology 51(1), 410-417.
- 523 Neta, P., Huie, R.E., Ross, A.B., 1988. Rate Constants for Reactions of Inorganic Radicals in
524 Aqueous Solution. Journal of Physical and Chemical Reference Data 17(3), 1027-
525 1284.
- 526 Paul, T., Dodd, M.C., Strathmann, T.J., 2010. Photolytic and photocatalytic decomposition of
527 aqueous ciprofloxacin: Transformation products and residual antibacterial activity.
528 Water Research 44(10), 3121-3132.
- 529 Serna-Galvis, E.A., Ferraro, F., Silva-Agredo, J., Torres-Palma, R.A., 2017. Degradation of
530 highly consumed fluoroquinolones, penicillins and cephalosporins in distilled water
531 and simulated hospital wastewater by UV254 and UV254/persulfate processes. Water
532 Research 122, 128-138.
- 533 Steele, W.V., Appelman, E.H., 1982. The standard enthalpy of formation of
534 peroxymonosulfate (HSO_5^-) and the standard electrode potential of the
535 peroxymonosulfate-bisulfate couple. The Journal of Chemical Thermodynamics 14(4),
536 337-344.
- 537 Takács-Novák, K., Noszál, B., Hermeecz, I., Keresztúri, G., Podányi, B., Szasz, G., 1990.
538 Protonation Equilibria of Quinolone Antibacterials. Journal of Pharmaceutical
539 Sciences 79(11), 1023-1028.
- 540 Van Doorslaer, X., Dewulf, J., Van Langenhove, H., Demeestere, K., 2014. Fluoroquinolone
541 antibiotics: An emerging class of environmental micropollutants. Science of the Total
542 Environment 500-501, 250-269.
- 543 Wang, P., He, Y.-L., Huang, C.-H., 2010. Oxidation of fluoroquinolone antibiotics and
544 structurally related amines by chlorine dioxide: Reaction kinetics, product and
545 pathway evaluation. Water Research 44(20), 5989-5998.
- 546 Wang, Z., Bush, R.T., Sullivan, L.A., Chen, C., Liu, J., 2014. Selective Oxidation of Arsenite
547 by Peroxymonosulfate with High Utilization Efficiency of Oxidant. Environmental
548 Science & Technology 48(7), 3978-3985.
- 549 Wols, B.A., Harmsen, D.J.H., Wanders-Dijk, J., Beerendonk, E.F., Hofman-Caris, C.H.M.,
550 2015. Degradation of pharmaceuticals in UV (LP)/H₂O₂ reactors simulated by means
551 of kinetic modeling and computational fluid dynamics (CFD). Water Research 75, 11-
552 24.
- 553 Xu, Y., Liu, S., Guo, F., Zhang, B., 2016. Evaluation of the oxidation of enrofloxacin by
554 permanganate and the antimicrobial activity of the products. Chemosphere 144, 113-
555 121.
- 556 Yang, B., Kookana, R.S., Williams, M., Ying, G.-G., Du, J., Doan, H., Kumar, A., 2016a.
557 Oxidation of ciprofloxacin and enrofloxacin by ferrate(VI): Products identification,
558 and toxicity evaluation. Journal of Hazardous Materials 320, 296-303.

559 Yang, Y., Banerjee, G., Brudvig, G.W., Kim, J.-H., Pignatello, J.J., 2018. Oxidation of
560 Organic Compounds in Water by Unactivated Peroxymonosulfate. *Environmental*
561 *Science & Technology* 52(10), 5911-5919.

562 Yang, Y., Pignatello, J.J., Ma, J., Mitch, W.A., 2016b. Effect of matrix components on
563 UV/H₂O₂ and UV/S₂O₈²⁻ advanced oxidation processes for trace organic
564 degradation in reverse osmosis brines from municipal wastewater reuse facilities.
565 *Water Research* 89, 192-200.

566 Yin, R., Guo, W., Wang, H., Du, J., Zhou, X., Wu, Q., Zheng, H., Chang, J., Ren, N., 2018.
567 Selective degradation of sulfonamide antibiotics by peroxymonosulfate alone: Direct
568 oxidation and nonradical mechanisms. *Chemical Engineering Journal* 334, 2539-2546.

569 Yun, E.-T., Lee, J.H., Kim, J., Park, H.-D., Lee, J., 2018. Identifying the Nonradical
570 Mechanism in the Peroxymonosulfate Activation Process: Singlet Oxygenation
571 Versus Mediated Electron Transfer. *Environmental Science & Technology* 52(12),
572 7032-7042.

573 Yun, E.-T., Yoo, H.-Y., Bae, H., Kim, H.-I., Lee, J., 2017. Exploring the Role of Persulfate in
574 the Activation Process: Radical Precursor Versus Electron Acceptor. *Environmental*
575 *Science & Technology* 51(17), 10090-10099.

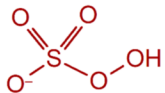
576 Zhang, H., Huang, C.-H., 2005. Oxidative Transformation of Fluoroquinolone Antibacterial
577 Agents and Structurally Related Amines by Manganese Oxide. *Environmental*
578 *Science & Technology* 39(12), 4474-4483.

579 Zhang, T., Chen, Y., Leiknes, T., 2016. Oxidation of Refractory Benzothiazoles with
580 PMS/CuFe₂O₄: Kinetics and Transformation Intermediates. *Environmental Science*
581 *& Technology* 50(11), 5864-5873.

582 Zhang, T., Zhu, H., Croué, J.P., 2013. Production of sulfate radical from peroxymonosulfate
583 induced by a magnetically separable CuFe₂O₄ spinel in water: Efficiency, stability,
584 and mechanism. *Environmental Science and Technology* 47(6), 2784-2791.

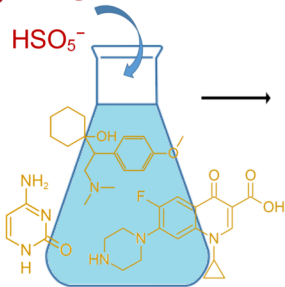
585 Zhou, Y., Gao, Y., Pang, S.-Y., Jiang, J., Yang, Y., Ma, J., Yang, Y., Duan, J., Guo, Q., 2018.
586 Oxidation of fluoroquinolone antibiotics by peroxymonosulfate without activation:
587 Kinetics, products, and antibacterial deactivation. *Water Research* 145, 210-219.

588

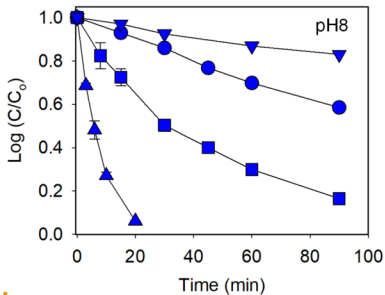


HSO_5^-

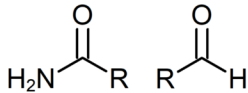
Kinetics: Piperazine moiety > Aliphatic amines
> Nitrogenous heterocyclic compounds



Nitrogenous Compounds



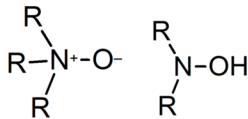
HRMS



R-NH_2

electron transfer

oxygen transfer



Transformation Products